Targeted activation in deterministic and stochastic systems

Bryan Eisenhower* and Igor Mezić
Department of Mechanical Engineering, University of California, Santa Barbara, CA, 93106 USA
(Received 13 October 2009; published 26 February 2010)

Metastable escape is ubiquitous in many physical systems and is becoming a concern in engineering design as these designs (e.g., swarms of vehicles, coupled building energetics, nanoengineering, etc.) become more inspired by dynamics of biological, molecular and other natural systems. In light of this, we study a chain of coupled bistable oscillators which has two global conformations and we investigate how specialized or *targeted* disturbance is funneled in an inverse energy cascade and ultimately influences the transition process between the conformations. We derive a multiphase averaged approximation to these dynamics which illustrates the influence of actions in modal coordinates on the coarse behavior of this process. An activation condition that predicts how the disturbance influences the rate of transition is then derived. The prediction tools are derived for deterministic dynamics and we also present analogous behavior in the stochastic setting and show a divergence from Kramers activation behavior under targeted activation conditions.

DOI: 10.1103/PhysRevE.81.026603 PACS number(s): 45.20.Jj, 05.45.−a, 45.50.Pk, 62.40.+i

A chain of strongly coupled oscillators, each of which is influenced by a multistable potential, can be viewed as a coarse representation of many physical systems which have more than one stable state or conformation from macromolecules to Josephson junctions and power grids. The transitions between these conformations are often observed in typical behavior (e.g., biomolecules) while at other times it is detrimental (e.g., extended power grids). Such transitions are often driven by stochastic influence (e.g., thermal noise), but in some cases, as in molecular systems, large local disturbances from the influence of enzymes, ligands, or other mechanical forces initiate the process [1,2]. Switching between these conformations typically follows one of two scenarios. In some cases, the states of the oscillators are weakly coupled which allows a few oscillators to go through excursions to a second stable state, eventually pulling the other oscillators along with them. In other cases, the oscillators may be strongly coupled, which forces the oscillator states to behave collectively and a coherent motion brings the entire chain over a global saddle at once [3]. In this paper, we investigate the second case, characterizing this global barrier with respect to local barrier heights, and consider different aspects of the transition process, including how the spatial structure of the disturbance influences the transition rate.

The Hamiltonian for an N oscillator system with a strong linear neighbor coupling (we will call this the backbone) and local nonlinearity takes the form

$$\mathcal{H} = \sum_{i=1}^{N} \frac{1}{2}\dot{q}_i^2 + \frac{1}{2}B(q_{i-1} - q_i)^2 + \varepsilon \mathcal{U}(q_i), \tag{1}$$

where $q_i \in \mathbb{R}$, B is the linear coupling strength, and ε is a small parameter. We will refer to this Hamiltonian for $\varepsilon = 0$ as the unperturbed or linear dynamics (note that all variables in this paper are real valued). For our analysis, the function $\mathcal{U}$ is a local bistable nonlinear potential. We have studied this function using a Morse potential acting on pendula in [3–5] where we compared the model to the dynamics of macromolecules and studied its qualitative behavior. The exponential form of the Morse potential makes analytical progress difficult, and so in this current study we investigate a 2–4 (or Duffing-type) potential to gain both qualitative and quantitative understanding of the phenomena. The 2–4 potential is:

$$\mathcal{U}(q_i) = -\left(\frac{1}{2}\delta q_i^2 - \frac{1}{4}q_i^4\right), \tag{2}$$

where δ is a constant that characterizes the distance between the two nonzero equilibria ($q_{eq} = \{0, \pm\delta\}$) and adjusts the curvature of the saddle which slightly alters the dynamics to better match the real behavior of proteins; see [6]. This potential has the same behavior as the Morse potential but is much easier to analyze. The backbone has periodic boundary conditions ($q_{N+1} = q_1$) and we have chosen the coupling strength in this backbone is much stronger than the local nonlinearity ($B \gg \varepsilon$). When this is the case the transition process is collective and coordinated (as described in [3]).

In Fig. 1 we present data from a simulation demonstrating such behavior using $\varepsilon = 1.0 \times 10^{-3}$, $\delta = 1$, and $B = 1$ (all numerical simulations in this paper were performed using a fourth-order symplectic method [7] with a fixed stepsize of 0.005). In this numerical experiment, we allow all but two oscillators to be at rest at the left equilibrium. Two of the oscillators are disturbed and this disturbance propagates through the oscillator chain, eventually bringing all the oscillators over their local saddle points (at $x = 0$) and into the right potential well. This transition process is very coherent as demonstrated by the collective motion which follows the mean of the oscillator positions.

In systems where the strength of the coupling is of the same order as the local nonlinearity, neighboring oscillators do not restrain each other from excursions across local barriers. These excursions, or *breathers*, initiate the transition process of the entire chain. In [8] it was shown that the transition process occurs when a set of small breathers merge into larger breathers with enough strength to pull the entire

*bryane@engr.ucsb.edu

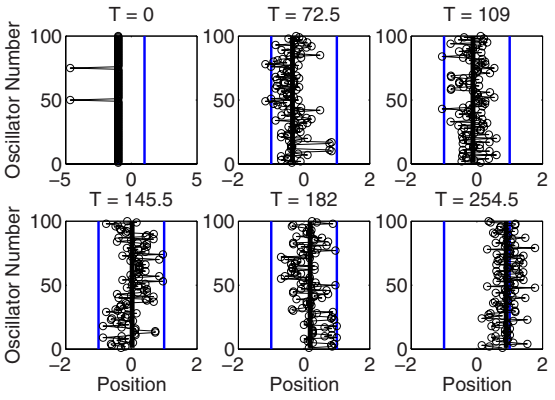

FIG. 1. (Color online) Snapshots of the evolution of 100 oscillators from one equilibrium (−1.0) to the other (1.0) in the potential (2) ($\varepsilon=1.0\times10^{-3}$, $\delta=1$, $B=1$). As a disturbance, two oscillators are perturbed. Because the coupling is much stronger than the nonlinearity, the transition is collective, closely following the mean (thick black line).

oscillator array over the barrier. In [9] the same research team developed an analytical calculation for the transition process by considering a single oscillator diffusing through a separatrix layer and subsequently pulling the other oscillators along. This theory does not work in our setting since the coupling strength is much greater than the local nonlinearity and excursion of a few oscillators and formation of breathers is discouraged. We find that it is not excursions of individual or groups of oscillators that drives the transition process, but rather dynamics of the mean position of all oscillators. In fact, we show that, in the averaged sense, the dynamics of the mean position and velocity of all oscillators are sufficient to predict specific quantitative properties of the activation process.

I. COORDINATE CHANGES

In order to gain insight into the qualitative or coarse behavior of this large system of coupled oscillators, we perform two canonical transformations. The first transformation projects the dynamics onto the Fourier modes of the backbone, which reveals a more global notion of the dynamics. We choose these coordinates because, due to the translational symmetry along the periodic chain, the normal basis consists of Fourier modes [10]. Because we are interested in the energy requirements for activation, we will then project the dynamics onto action-angle coordinates. This will not only highlight the energetic behavior within the modes, it will also provide a system which is well suited for averaging which will be performed in Sec. III.

We perform the canonical transformation onto modal coordinates using

$$q_i = \sqrt{\frac{2}{N}} \sum_{k=1}^{N/2-1} \left[\frac{\hat{q}_0}{\sqrt{2}} + \cos(2\pi ik/N)\hat{q}_k + \frac{\cos(\pi k)}{\sqrt{2}}\hat{q}_{N/2} + \sin(2\pi ik/N)\hat{q}_{N/2+k} \right], \tag{3}$$

where $\hat{q}_k$ are modal amplitudes and k is the wavenumber. The

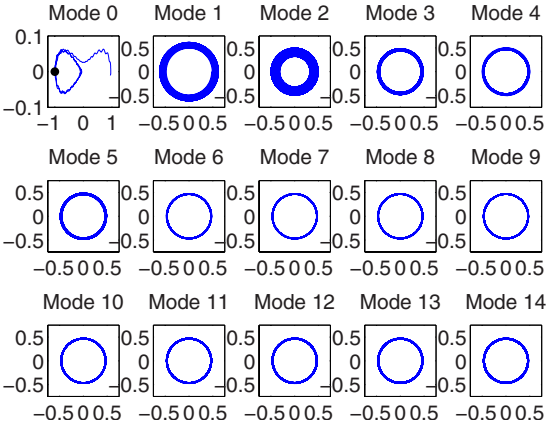

FIG. 2. (Color online) Example numerical simulation in modal coordinates. Each subplot shows the state space of the first 15 modes (the modal amplitude and its time derivative). The upper left subplot is the zeroth mode illustrating all oscillators in transition from one potential well to the other. The initial condition of the zeroth mode is the large dot. The trajectories in the lower modes (1 and 2) are growing in radius for this particular simulation.

transformation rules from velocities $\dot{q}_i$ to modal velocities $\dot{\hat{q}}_k$ are obtained from time differentiation of Eq. (3). The zeroth mode $\hat{q}_0$ is the averaged coordinate (scaled by $\sqrt{N}$) and the coordinates $\hat{q}_{1\ldots N/2-1}$ are typical spatial Fourier modes. This transformation is very similar to the one from [11], although since in this case since the chain has a periodic backbone, only full Fourier modes are considered.

The transformation (3) is just a projection of the dynamics onto the orthonormal eigenvectors of the unperturbed Hamiltonian ($\varepsilon=0$). Collecting these vectors into a matrix $\mathcal{M}$ which is real, symmetric, and orthonormal (the same matrix is used in [5]), we have the Hamiltonian in modal coordinates:

$$\mathcal{H}(\hat{\vec{q}},\dot{\hat{\vec{q}}}) = \frac{1}{2}\dot{\hat{\vec{q}}}^T\dot{\hat{\vec{q}}} + B\hat{\vec{q}}^T\Omega\hat{\vec{q}} + \varepsilon U(\mathcal{M}^T\hat{\vec{q}}), \tag{4}$$

where Ω is a square matrix with the linear frequencies on its diagonal. These real nonzero frequencies $\vec{\omega} = \|\sqrt{2-2\cos(2k\pi/N)}\|$, $k=1,2,\ldots,N-1$ of the unperturbed Hamiltonian start at zero, increase nearly linearly near zero and collect at 2.0 as k grows large.

We present a second numerical experiment in Fig. 2 using the same parameters as in Fig. 1, but in this case the simulation is performed in modal coordinates. Unlike the experiment in Fig. 1, the zeroth mode is placed at its equilibrium meaning that there is no tendency of the mean away from the initial potential well, but all other nonzero modes are disturbed. The disturbance in these nonzero modes eventually influences the zeroth mode, driving it off its equilibrium and eventually forcing a transition to the other potential well.

In Fig. 2, the structure of a system which has one highly nonlinear state coupled to many nearly linear (integrable) oscillators is evident. In the upper left subplot the state space of the zeroth mode is shown, illustrating that during the activation process, the mean of the oscillator positions travels from one potential well to the other. It is also clear that the

response of the other modes is nearly linear by observing nearly periodic, circular orbits in each of their own state spaces, which is expected because $\varepsilon \ll B$.

The system studied in this paper fits into the class of nonlinear systems which is close to a coupled chain of linear harmonic oscillators. Such near-integrable systems have been studied in [12], where equipartition of energy and dynamic properties related to integrable instability theory of partial differential equations were investigated (see also [13]). In particular, systems like this lend themselves to analysis in action-angle coordinates [14] which highlight the energy and frequency dependencies in each coordinate while also characterizing adiabatic invariants. With this in mind, we perform a second canonical transformation into action-angle coordinates using the following rules for nonzero wavenumbers k:

$$\hat{q}_k = \sqrt{\frac{2J_k}{\omega_k}} \sin \phi_k, \quad \hat{\dot{q}}_k = \sqrt{2J_k\omega_k} \cos \phi_k. \tag{5}$$

For notational convenience we rename $\hat{q}_0 \to x$ and $\hat{\dot{q}}_0 \to y$, and the resulting system takes the form

$$\dot{x} = y, \quad \dot{\phi}_k = \omega_k + \varepsilon f_k(x, \vec{J}, \vec{\phi}),$$

$$\dot{y} = \varepsilon g_0(x, \vec{J}, \vec{\phi}) \quad \dot{J}_k = \varepsilon g_k(x, \vec{J}, \vec{\phi}), \tag{6}$$

for $k = 1, 2, \ldots (N-1)$, where ϕ_k are angle variables and J_k are the conjugate actions.

The same simulation which was presented in Fig. 2 is illustrated in action-angle coordinates in Fig. 3. In this figure we see that as the transition process proceeds (x going from less than to greater than zero at $t \approx 8800$), the change in angles (frequencies) are nearly constant within the resolution of the plot. In addition to this, we find that actions do change but in a stepwise fashion. We find that the actions change predominantly when the position of the zeroth mode approaches -1.0, which is a zone of resonance for the system. The approximate locations of the resonance zones are labeled with the letter "R." Both of these behaviors are a testament to the near-integrability of the dynamics.

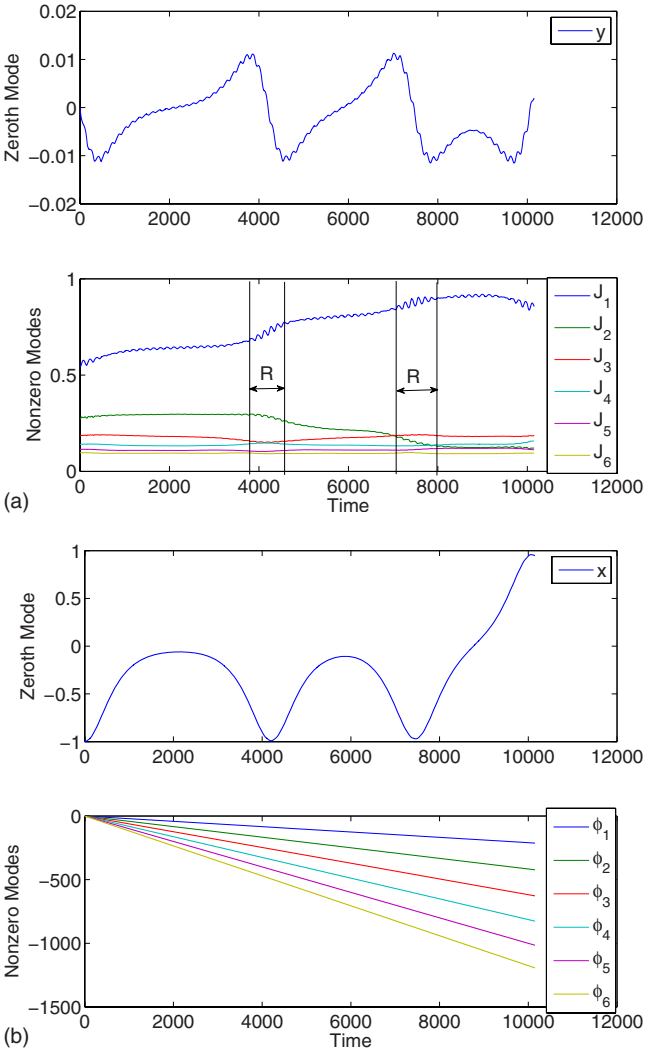

FIG. 3. (Color online) Example numerical simulation in action-angle coordinates (same parameters and initial conditions as Fig. 2). The upper two subplots illustrate the nonzero actions (and momentum of the zeroth mode), while the lower two subplots illustrate the position of the zeroth mode and conjugate angles of the nonzero actions.

II. INTERNAL RESONANCE

As we have mentioned, resonance is a key factor in the transition process, as it is a pathway for energy transfer in coupled oscillators with similar frequencies. When these oscillators are nonlinear, with frequencies that change with the amplitude of oscillation, resonance becomes a time-dependent phenomenon. That is, as the system evolves it may pass in and out of resonance or even become trapped in resonance (see [15] for a description of complex resonance phenomena). We are interested in resonance for two reasons: (1) it is a means for energy transfer which takes energy from any disturbance on the oscillators to the transition between the two potential wells and (2) we wish to perform time averaged analysis of the dynamics by the use of averaging which itself is sensitive to resonance, and therefore we need to be familiar with this behavior.

The resonance condition for a multifrequency system is [16]:

$$|(\vec{\kappa}, \vec{\omega})| < \frac{1}{c|\vec{\kappa}|^{\upsilon}}, \tag{7}$$

where $(\vec{\kappa}, \vec{\omega}) = \kappa_0\omega_0 + \kappa_1\omega_1 + \cdots + \kappa_{N-1}\omega_{N-1}$, $\kappa_k \in \mathbb{Z}\backslash\{0\}$, and c, υ are positive constants. The quantity on the left-hand side of the inequality goes to zero when frequencies become rationally commensurate. The term on the right-hand side accounts for resonance in small regions where the frequencies are almost commensurate. In fact the size of the *resonance zone*, both in phase space dimension and time spent inside, is related to this value.

The linear modal frequencies of the unperturbed Hamiltonian are not commensurate in our system and therefore there is no energy exchange between modes when $\varepsilon = 0$.

However, when $\varepsilon \neq 0$ there are regions in the state space where the nonlinearity becomes very important. It is in these regions that the frequencies begin to change and resonance occurs. This resonance is important as it allows energy to be transmitted from any disturbance to the collective motion, leading to the transition or conformation change [3]. We will specifically discuss the direction of energy transfer or *funneling* in Sec. V.

Not only does the presence of multiple frequencies enhance energy transfer, it also complicates the analysis of any system, including the use of tools such as averaging. In summary, similar frequencies introduce small denominators, which influences the stability of the dynamics. In addition to this, resonance alters or destroys adiabatic invariants. In the case where a pair or more of frequencies are commensurate in an m-frequency system, the trajectories of the unperturbed motion fill a torus with a dimension smaller than m, so averaging over the original torus will not capture the dynamics correctly. That is, the previously dense set of angle trajectories falls onto a smaller set (subtorus) in the resonant case. The general idea of how to deal with resonance during averaging is to make a canonical change of variables onto to a coordinate system that rotates along with the resonant frequency and therefore capture only the slow variation around this frame of reference. Alternatively, in the case where only some of the frequencies are resonant the method of partial averaging [16] is employed. In partial averaging, the vector of angles is parsed into resonant and nonresonant angles and averaging is performed using only the nonresonant variables.

III. AVERAGING

In the present study, we perform partial averaging over the nonzero modes to gain an imperfect reduced representation of the dynamics. Generally, averaging will offer a reduced model of dynamics in certain time or spatial ranges; here our reduced order representation will represent the dynamics well only outside of resonance. To obtain a coarse representation we average over the angle variables of M nonzero modes ($M \leq N$ as the analysis can be performed on a reduced order model since the transformations are canonical). The averaged Hamiltonian becomes

$$\overline{\mathcal{H}}(x,y,\vec{J}) = \frac{1}{(2\pi)^M}\int_0^{2\pi}\cdots\int_0^{2\pi}\mathcal{H}(x,y,\vec{J},\vec{\phi})d\phi_1\ldots d\phi_M. \tag{8}$$

For the specific 2–4 potential the resulting averaged oridinary differential equation (ODE) derived from Hamilton's equations is

$$\dot{\bar{x}} = \bar{y}, \quad \dot{\bar{y}} = \varepsilon\left(\delta - \frac{3}{N}\sum_{k=1}^{M}\frac{\bar{J}_k}{\omega_k}\right)\bar{x} - \frac{\varepsilon\bar{x}^3}{N}. \tag{9}$$

In an averaged sense, actions in the higher modes are stationary in time ($\dot{\bar{J}}_k = 0,\ k \geq 1$) and feed into the zeroth mode dynamics. In this sense, Eq. (9) represents dynamics induced by a parametric 2–4 potential for the planar variables (x,y), where higher order actions $(\bar{J}_k, k = 1,2,\ldots,M)$ alter the existence and location of the equilibrium branches.

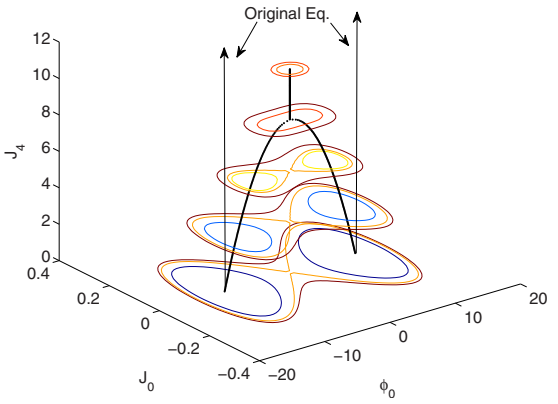

FIG. 4. (Color online) Impact of energy in higher order modes (e.g., J_4) on the zeroth mode, illustrating how the *original* equilibria are moved outside of the libration state to the rotation state.

There is a dependency between the activation rate and the amount of disturbance energy (and in particular, the spatial character of the disturbance energy) which can be captured quantitatively using the averaged model (9). In the averaged sense, the zeroth mode has the typical figure-eight phase space of the 2–4 potential with equilibria at $\bar{x}_{eq} = \pm\sqrt{N\delta}$. If all oscillators are at rest so that the zeroth mode is at this equilibrium, and there is no energy in higher modes, no oscillations will occur. As soon as energy from a higher mode is introduced the oscillators will begin to oscillate. In fact, the mean (zeroth mode) begins to oscillate as well. This phenomenon is captured in the averaged model by a shift in the equilibria of the zeroth mode. In fact, the equilibria shift toward the origin, bringing the separatrix closer to the initial location of the zeroth mode. With sufficient energy in any one of these higher order modes, the separatrix of the zeroth mode will be driven closer to the origin, and eventually the original location of the zeroth mode will breach it. When this occurs the zeroth mode will be forced into the rotation state and transition to the second equilibrium will occur. This concept is illustrated in Fig. 4.

With this in mind, the minimum activation energy becomes the amount of energy needed from the higher mode(s) to pull the separatrix over the original equilibrium location $\bar{x}$ (this occurs when $J_4 = 4.1783$ for the example in Fig. 4). The activation condition is

$$\overline{\mathcal{U}}(\bar{x} = 0.0, \vec{J}) = \overline{\mathcal{U}}(\bar{x} = \bar{x}_{eq}, \vec{J}), \tag{10}$$

which defines the minimum activation energy for transition. Performing the necessary calculations, the resulting activation condition for the 2–4 potential becomes

$$\sum_{i=1}^{M}\frac{\bar{J}_i}{\omega_i} = \frac{\delta N}{6}, \tag{11}$$

which describes an affine hyperplane with a dimension equal to the number of nonzero actions. It is evident in Fig. 4 that with further increase of action in the higher modes, the two wells disappear, and the zeroth mode will repetitively circle both original equilibria in a state of rotation. Indeed a pitch-

fork bifurcation exists for these high energy orbits at $\Sigma_{i=1}^{M}\frac{\bar{J}_i}{\omega_i}=\frac{\delta N}{3}$ which is twice the minimum activation energy (for the example in Fig. 4 this occurs at $J_4=8.3567$). It is known that in this region parametric resonance occurs which brings completely new phenomena [17]. This has not been studied in this paper as we focus on low energy transitions at the present time.

A summary of the activation process is as follows: as the system evolves from any initial condition, energy transfer occurs between the modes as it passes through resonance. Once this passage is complete, if the actions meet condition (11), the system will escape from its initial well and transition to the second well. Passage through resonance will continue to occur once it is in the second well and in many cases the energy will be dispersed through the modes once again. If the condition (11) is met again, the system will re-escape and return to its initial potential well. If not, it will continue to librate in the second well.

To calculate the full activation time vs. activation energy profile we note that the when the oscillation of the zeroth mode is in its rotation state, the activation time is the time in which the trajectory crosses $\bar{x}=0.0$. In fact, since the figure-eight phase space for the rotation state is symmetric, this is 1/4 of the period of a rotation state. We can analytically derive the rate of activation by calculating the period of rotation oscillations of the zeroth mode in Eq. (9) as it is parametrically altered by higher wavenumber actions. To calculate the period of under a single-mode perturbation we write the Hamiltonian of the averaged dynamics as

$$\mathcal{H}(\bar{x},\bar{y},\bar{\vec{J}})=\frac{\bar{y}^2}{2}-\left(\frac{a\bar{x}^2}{2}+\frac{b\bar{x}^4}{4}\right),$$

$$a=\varepsilon\left(\delta-\frac{3\bar{J}_i}{\omega_i N}\right),\quad b=-\frac{\varepsilon}{N}. \tag{12}$$

This system admits an analytical solution that is different inside and outside of the figure-eight separatrix. On the outside of the separatrix we calculate the period as

$$T_{out}=\frac{4K(\kappa)}{\omega_{out}},$$

$$\text{where}\quad \kappa=\frac{\bar{x}(0)\sqrt{b}}{\sqrt{2(a+b\bar{x}(0)^2)}},\quad \omega_{out}=\frac{\sqrt{a}}{\sqrt{2\kappa^2-1}}, \tag{13}$$

where κ is the elliptic modulus and $K(k)$ is the complete Jacobi elliptic integral of the first kind. The variable $\bar{x}(0)$ is the amplitude of the initial condition of the zeroth mode [$\bar{x}(0)=-\sqrt{N\delta}$ for the previous discussions].

For comparison, numerical data was generated using $N=100$ oscillators, $B=1$, $\varepsilon=0.001$, and $\delta=1$ and is presented in Fig. 5. The analytical expression captures numerical data well when the activation rates exceed the modal frequencies; the discrepancy in lowest mode at high activation rates is because the modal frequency (over which we average over) approaches the activation rate itself.

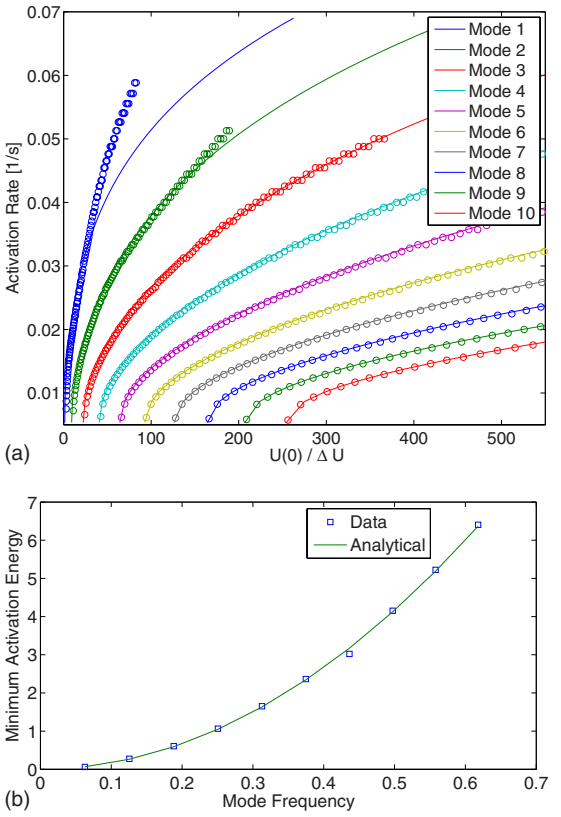

FIG. 5. (Color online) Activation energy vs rate (top) and minimum activation energy (bottom). Analytical—solid, numerical simulation—discrete points. $\Delta U=\frac{\varepsilon N\delta}{4}$ is the sum of the barrier heights and $U(0)$ is the initial disturbance.

IV. COMPARISON WITH STOCHASTIC ACTIVATION

The results presented above for activation in networks of coupled oscillators in a noise free environment are new results in this field. On the other hand, prediction tools for noise assisted activation have been available for some time. There are results from nonequilibrium statistical mechanics that predict the stochastic activation rates for oscillators experiencing Brownian motion in a metastable environment, termed *escape rate theory* (see a thorough review in [18]). Escape rate theory characterizes the transition process of an inertial mass from a *reactant* well across a high energy barrier or saddle. The predominant question in rate theory is to determine how fast particles make the transition from the reactant to product state when excited by thermal noise. The theoretical analysis of escape rates began in the 1880s with Arrhenius, who from experimental results of chemical reactions found that the rate of a chemical reaction took an exponential form depending on the barrier height, amount of excitation, and an unknown prefactor. In the 1940s, Kramers offered new insight into the analytical derivation of this prefactor by studying a particle moving in a one-dimensional bistable potential adhering to Brownian motion. This motion is described by Langevin dynamics and the diffusion of probability density is described by the Fokker-Planck equation.

The results for stochastic transitions that Kramers derived are associated with the activation dynamics of systems which

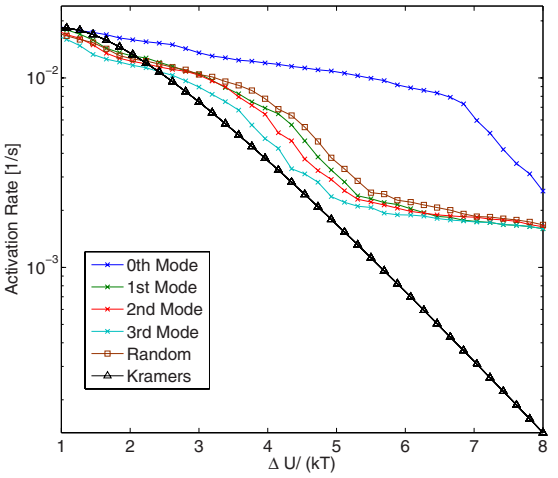

FIG. 6. (Color online) Stochastic simulation with targeted perturbation in the first 4 Fourier modes compared to a random disturbance condition. These rates are compared to the Kramers estimate.

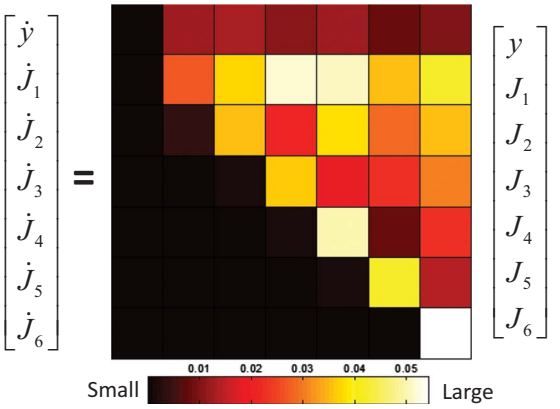

FIG. 7. (Color online) Absolute value of the time averaged Jacobian of action variables illustrating the funneling of energy toward the lowest mode.

can be described by one reaction coordinate. Any other modes in the dynamics are assumed to not influence the transition process or are lumped into the dynamics of the thermal bath. Our interest, motivated from engineering examples and some biological examples, is of networked systems with a strong backbone. Because of this strong backbone, as we have shown in the previous sections of this paper, the Fourier modes play an important part in the activation process. Below we intend to show how these modes influence the stochastic transition and the rate predictions from the Kramers formula.

In order to do this, Langevin simulations were performed on Eqs. (1) and (2) to determine if the presence of disturbance energy in different modes influences the rate. In Fig. 6 we illustrate the stochastic rates using the same parameters as before with a Langevin damping value of 0.05. In this case we impose a disturbance energy at a constant value of $5\Delta U$ in different spatial patterns, including a randomly selected series of positions. The data is simulated for different temperatures (Boltzmann's constant $k=1.0$) and compared to the Kramers estimate for low damping (see Eq. 4.49 of [18]). We find that at higher temperatures, the Kramers theory predicts the behavior well, while at lower temperatures inertia dominates and the numerical data diverges from the Kramers estimates. The faster rates observed in the numerical data for low temperatures may be due to a collective phenomena from the coupling of the large number of oscillators. With respect to targeted disturbance, there is a clear distinction in the stochastic rate when influenced by these disturbances which is not accounted for in Kramers' original work. The reason for presenting these results is not to provide analytical or numerical tools, but rather to highlight the basic phenomenological behavior of the stochastic transition of Eq. (1) and to illustrate limitations in Kramers theory that should be acknowledged when studying similar systems.

V. SELECTIVE PARTITIONING OF ENERGY

Above we have been able to predict a *static* relationship between disturbance energy and activation time. However, the transfer of energy from modes which contain disturbance energy (higher modes) to the zeroth mode is a dynamical process. The equal balance of modal energy (equipartition) is expected in many high dimensional systems due to ergodicity, but is not always the case. As shown initially by Fermi, Pasta, and Ulam [11] this balance of energy may not occur even for relatively simple dynamics. In fact, Ford later illustrated that this lack of energy balance is due to a lack of commensurate temporal frequencies in the set of spatial modes, and its consequence, the KAM theorem [19]. As we have mentioned, the frequencies of the linear normal modes in our model are incommensurate. Without any nonlinear perturbation to the backbone, we expect there to be no resonance (energy transfer) at all. However as we have shown, there is no doubt that energy transfer occurs because activation can be observed by global motions of the zeroth mode and this is realized by imposing a disturbance on modes of high wavelength. In fact, the energy transfer does not lead to equipartition immediately, rather it follows a unidirectional route to the lowest mode as the system passes through zones of resonance.

By calculating the Jacobian of Hamilton's equations for the action-angle system (6) we obtain a matrix that reveals the change in action variables as influenced by other actions and angles. It turns out that the change in action is mostly dependent on other actions (as opposed to angles); we present this submatrix in Fig. 7 for an example simulation with seven modes. We see that the change in action in any particular mode is dominated by influences of modes of equal or higher wavenumber only. This natural funneling of energy is remarkable and strengthens the robustness of the transition process. In fact, the funneling concept is associated with the horizontal-vertical graph theoretic structure of the dynamics, which has been shown to be a way to characterize the robustness of a dynamical system [20].

VI. SUMMARY

We have found that even though this high dimensional system uses a complex nonlinear process to achieve global

transition between different states, the qualitative nature is easily understood as a funneling of energy from higher modes to the lowest mode, whose phase space dynamics is manipulated by these higher modes. In fact the dynamics of the zeroth mode parameterized in an averaged sense by dynamics of the the higher modes are enough to predict the activation process. These results were also compared to the stochastic setting and it was shown that the spatial character of the perturbation influences the divergence from the Kramers estimate.

ACKNOWLEDGMENTS

This work was supported in part by DARPA DSO under AFOSR contract No. FA9550-07-C-0024, and AFOSR Grants No. FA9550-06-1-0088 and FA9550-09-1-0141.

[1] S. Cocco, R. Monasson, and J. Marko, Proc. Natl. Acad. Sci. U.S.A. **98**, 8608 (2001).
[2] F. Piazza and Y.-H. Sanejouand, Phys. Biol. **5**, 026001 (2008).
[3] I. Mezić, Proc. Natl. Acad. Sci. U.S.A. **103**, 7542 (2006).
[4] B. Eisenhower and I. Mezić, Proceedings of the 46th IEEE Conference on Decision and Control, New Orleans 2007 (unpublished).
[5] P. Du Toit, I. Mezíć, and J. Marsden, Physica D **238**, 490 (2009).
[6] S. Lee and W. Sung, Phys. Rev. E **63**, 021115 (2001).
[7] H. Yoshida, Phys. Lett. A **150**, 262 (1990).
[8] P. Hänggi, L. Schimansky-Grier, and P. Hanggi, Europhys. Lett. **78**, 20002 (2007).
[9] P. Hänggi, S. Fugmann, L. Schimansky-Geier, and P. Hanggi, Acta Phys. Pol. B **39**, 1125 (2008).
[10] J. Lumley, P. Holmes, and G. Berkooz, *Turbulence, Coherent Structures, Dynamical Systems and Symmetry* (Cambridge University Press, London, 1996).
[11] E. Fermi, J. Pasta, and S. Ulam, Los Alamos Report No. LA-1940 (1955).
[12] M. G. Forest, C. G. Goedde, and A. Sinha, Phys. Rev. Lett. **68**, 2722 (1992).
[13] N. Ercolani, M. G. Forest, and D. W. McLaughlin, Physica D **43**, 349 (1990).
[14] H. Goldstein, *Classical Mechanics*, 6th ed. (Addison-Wesley, London, 1959).
[15] D. Vainchtein, A. Neishtadt, and I. Mezić, Chaos **16**, 043123 (2006).
[16] *Dynamical Systems III*, edited by V. Arnol'd (Springer-Verlag, New York, 1988).
[17] E. Shlizerman and V. Rom-Kedar, Phys. Rev. Lett. **102**, 033901 (2009).
[18] P. Hänggi, P. Talkner, and M. Borkovec, Rev. Mod. Phys. **62**, 251 (1990).
[19] J. Ford, J. Math. Phys. **2**, 387 (1961).
[20] I. Mezić, 43rd IEEE Conference on Decision and Control 2004 (unpublished).